Infrared Spectra and Theoretical Calculations of Lithium Hydride Clusters in Solid Hydrogen, Neon, and Argon

Xuefeng Wang and Lester Andrews*

Department of Chemistry, P.O. Box 400319, University of Virginia, Charlottesville, Virginia 22904-4319

Received: February 13, 2007; In Final Form: April 13, 2007

A matrix isolation IR study of laser-ablated lithium atom reactions with H_2 has been performed in solid *para*-hydrogen, normal hydrogen, neon, and argon. The LiH molecule and $(LiH)_{2,3,4}$ clusters were identified by IR spectra with isotopic substitution (HD, D_2, and $H_2 + D_2$) and comparison to frequencies calculated by density functional theory and the MP2 method. The LiH diatomic molecule is highly polarized and associates additional H_2 to form primary $(H_2)_2LiH$ chemical complexes surrounded by a physical cage of solid hydrogen where the ortho and para spin states form three different primary complexes and play a role in the identification of the bis-dihydrogen complex and in characterization of the matrix cage. The highly ionic rhombic $(LiH)_2$ dimer, which is trapped in solid matrices, is calculated to be 22 kcal/mol more stable than the inverse hydrogen bonded linear LiH−LiH dimer, which is not observed here. The cyclic lithium hydride trimer and tetramer clusters were also observed. Although the spontaneous reaction of 2 Li and H_2 to form $(LiH)_2$ occurs on annealing in solid H_2, the formation of higher clusters requires visible irradiation. We observed the simplest possible chemical reduction of dihydrogen using two lithium valence electrons to form the rhombic $(LiH)_2$ dimer.

Introduction

Lithium hydrides are ideal hydrogen storage materials because of their very large hydrogen mass percentage, and the ternary lithium hydrides ($LiBH_4$, $LiAlH_4$, Li_3AlH_6, etc.) have been explored as new efficient storage materials.[1−3] The discovery of catalyst supported lithium aluminum hydrides gave promising reversibility for hydrogen storage.[4,5] New reactions of LiH with metal amides have also provided a source of hydrogen.[3,6,7] Since LiH is the smallest heteronuclear diatomic molecule (except the dihydrogen isotope HD), it has been studied extensively both theoretically and experimentally.[8−18] The equilibrium partial pressure of LiH is low in the gaseous elements at high temperature,[8] and accordingly, there is no experimental evidence for LiH clusters. Solid LiH forms the stable cubic NaCl crystal structure.[19] Lithium hydride anions have been investigated in the gas phase by photoelectron spectroscopy.[12] The small Li_nH molecules have been identified in mass spectrometric measurements, and their stability and structure have been studied with density functional and large coupled-cluster computations.[20,21]

The hydrogen bond is well-known to play a key role in the structure and functions of water and biological molecules. Recently, a new type of hydrogen bond, the inverse hydrogen bond, was suggested in which one electronegative hydrogen provides electrons and another electropositive non-hydrogen or hydrogen accepts them.[17] The linear Li−H−Li−H dimer is the simplest model for this type of complex.[18] Theoretical calculations have been performed for lithium hydride dimers in a number of earlier studies, and the rhombic dimer is about 22 kcal/mol lower in energy than the linear dimer.[14] Lithium is the closest congener of hydrogen, and the lithium bond has been proposed as an analogue with hydrogen bonding, and comparisons have been made.[22]

Recently, we reported the preparation of dialane (Al_2H_6) using the reaction of laser-ablated aluminum with pure H_2 during condensation at 3.5 K.[23] The AlH generated from laser ablation further reacts with H_2 to give AlH_3 with UV photolysis, which dimerizes to form Al_2H_6. Further evidence shows trialane (Al_3H_9) and tetraalane (Al_4H_{12}) to be stable molecules. Similarly, metal hydrides have also been investigated for group 2, 12, and 13 metals in solid hydrogen.[24−26]

In this paper, we present a search for lithium hydride clusters in low-temperature matrices. Lithium atoms have been investigated in noble gas and hydrogen solids through electronic absorption spectra.[27,28] The more recent hydrogen matrix work suggested that some incident lithium atoms may react but that no lithium hydride products could be identified from the electronic spectrum. Infrared spectra were employed here to collect molecular vibrational information, and theoretical calculations were used to predict molecular spectroscopic and structural properties to support the experimental work. *Para*- and *ortho*-hydrogen mixtures were used to characterize the (H_2)-LiH complex. We have discovered that annealing allows Li atoms to diffuse and react in solid hydrogen to form rhombic $(LiH)_2$, which has been reported in a preliminary communication.[29]

Computational Methods

The methods for investigating laser-ablated metal atom reactions with hydrogen in excess molecular hydrogen, neon, or argon during condensation at 4 or 8 K have been described in detail previously.[23,30] The Nd:YAG laser fundamental (1064 nm, 10 Hz repetition rate with 10 ns pulse width) was focused (spot diameter 0.1 mm) onto a rotating lithium metal target ^nLi (Fisher, rod, 92.6% ^7Li, 7.4% ^6Li) and ^6Li (Oak Ridge National Lab, 95.6% ^6Li, 4.4% ^7Li). The targets were washed with hexane, scraped to expose a fresh surface, and transferred to
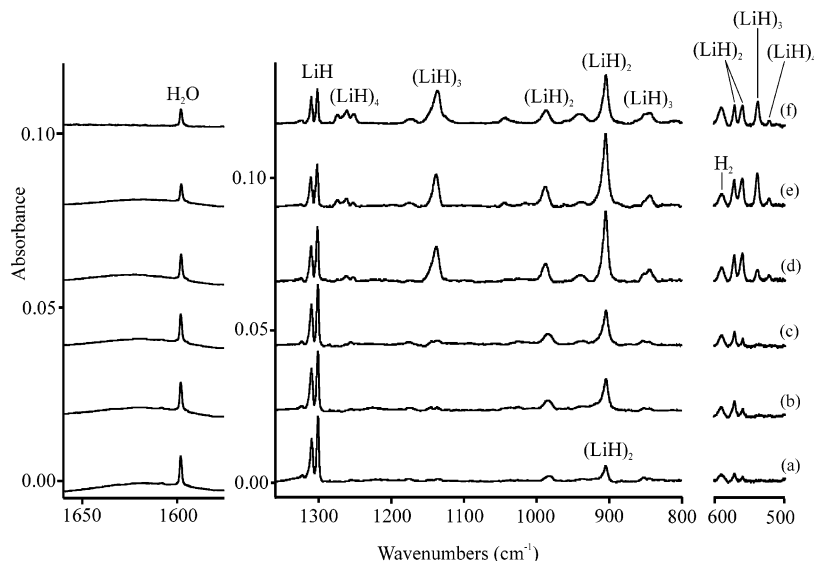

Figure 1. Infrared spectra in selected regions for lithium atom reaction products with hydrogen. (a) Spectrum after co-deposition of laser-ablated natural isotopic lithium atoms and hydrogen for 30 min at 4 K, (b) after annealing to 6.5 K, (c) after annealing to 6.8 K, (d) after >520 nm irradiation, (e) after >290 nm irradiation, and (f) after annealing to 7.3 K.

the vacuum chamber. The laser energy was varied in a low range to avoid forming metal clusters (typical energy about $1-3$ mJ/pulse). Reagent isotopic substitution [HD (97.9% HD, 2.0% H_2, 0.05% D_2), D_2, $H_2 + D_2$] was employed. Samples of *para* or *ortho* enriched H_2 or D_2 were also investigated.[31] FTIR spectra were recorded at 0.5 cm^{-1} resolution on Nicolet 750 with 0.1 cm^{-1} accuracy using an MCTB detector. Matrix samples were annealed at different temperatures, and selected samples were subjected to 10 min irradiations by a medium-pressure mercury arc lamp (Philips, 175W) with the globe removed using glass optical filters. Complementary DFT calculations were performed using the Gaussian 03 program system, the B3LYP density functional, and the 6-311+G(3df,3pd) basis set. Additional MP2, CCSD(T), and QCISD calculations were performed for comparison.[32] Calculated reaction energies include zero point vibrational corrections.

Results

Infrared spectra are presented for lithium atom reaction products with H_2, D_2, HD, and a $H_2 + D_2$ mixture in excess pure normal molecular hydrogen, HD, and deuterium. Absorptions common to hydrogen matrix experiments, namely, $H(H_2)_n$, $H^-(H_2)_n$, and $D_3^+(D_2)_n$,[33] have been reported previously and are not discussed here. Similar experiments have been performed in *para*-hydrogen and *ortho*-deuterium enriched samples[31,34] for comparison and identification of the bis-dihydrogen complex. Neon and argon matrix investigations will also be reported. Extensive DFT and MP2 theoretical calculations of lithium hydride clusters and hydrogen complexes were performed to support identification of the experimental observations.

Infrared Spectra. Matrix spectra of laser-ablated lithium atom reaction products in pure normal H_2 formed during co-deposition at 4 K revealed new bands at 1309.9, 1301.2, 904.7, 981.4, 571.2, and 559.8 cm^{-1}. Photolysis with >520 nm irradiation decreased the 981.4 cm^{-1} absorption, increased the 904.7, 571.2, and 559.8 cm^{-1} bands by a factor of 4, and generated new bands at 1138.0, 987.1, 538.9, and 522.3 cm^{-1}, while the 1309.9 and 1301.2 cm^{-1} bands decreased slightly. Infrared spectra from another experiment are shown in Figure 1, where first annealing to 6.5 and to 6.8 K after deposition doubled the absorptions labeled (LiH)$_2$. Subsequent >630 nm
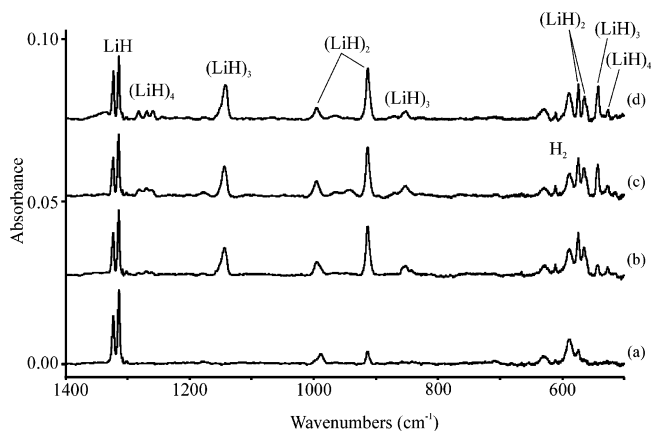

Figure 2. Infrared spectra in selected regions for lithium atom reaction products with hydrogen. (a) Spectrum after co-deposition of laser-ablated lithium-6 atoms and hydrogen for 30 min at 4 K, (b) after >520 nm irradiation, (c) after >380 nm irradiation, and (d) after annealing to 7.0 K.

irradiation, which covers the Li atomic absorption, had no effect on the spectrum, but >520 nm irradiation, which overlaps the low-energy side of the Li_2 absorption, doubled the (LiH)$_2$ bands and produced the new bands given previously. Further >290 nm irradiation slightly reduced the previous product absorptions and increased a trio of bands at 1274.4, 1261.8, and 1252.2 cm^{-1} (labeled (LiH)$_4$) (Figure 1e). Annealing to 7.3 K further reduced the previous absorptions, increased the trio (Figure 1f), and removed 10% of the hydrogen sample based on the absorption near 4150 cm^{-1}. Further sample warming removed all absorptions. Experiments were also performed reversing the order of annealing and irradiation, and the product growth on irradiation was the same as shown in Figure 1, but the growth of (LiH)$_2$ bands on subsequent annealing was only 20% as much. Analogous reactions with ^{6}Li gave similar spectra with appropriately shifted bands as illustrated in Figure 2. Lower laser energy was employed in another ^{6}Li experiment with H_2, and the 1323.1 and 1314.1 cm^{-1} bands were weaker, but the 913.3 cm^{-1} absorption increased by a factor of 4 on annealing to 5.5−6.5 K and a factor of 2 on >520 nm irradiation.

In solid normal deuterium with ^{7}Li, the upper bands shifted to 977.8, 852.8, 748.0, and 691.0 cm^{-1}, and ^{6}Li atom reactions
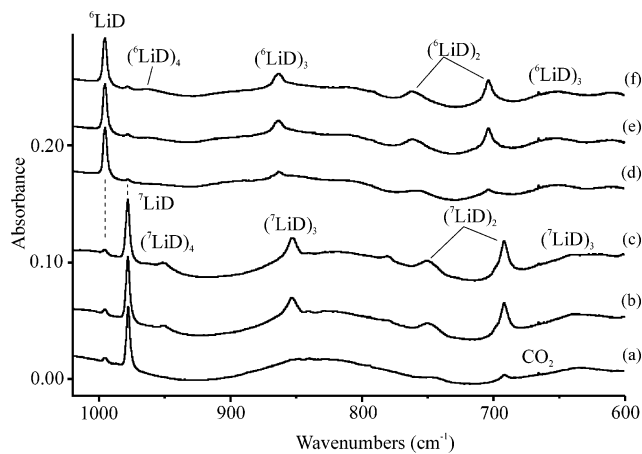
Figure 3. Infrared spectra in selected regions for lithium atom reaction products with deuterium. (a) Spectrum after co-deposition of laser-ablated natural isotopic lithium atoms and D_2 for 30 min at 4 K, (b) after >470 nm irradiation, and (c) after >290 nm irradiation. (d) Spectrum with ^6Li and D_2, (e) after >520 nm irradiation, and (f) after >380 nm irradiation.
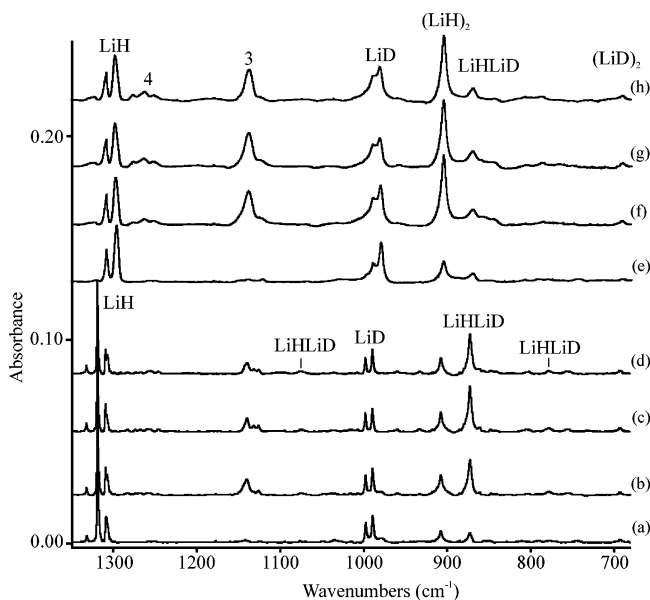

Figure 4. Infrared spectra in the 1350−680 cm^{-1} region for Li atom reaction products with mixed H and D reagents. (a) Spectrum after co-deposition of laser-ablated natural isotopic Li atoms and HD for 30 min at 4 K, (b) after >470 nm irradiation, (c) after >290 nm irradiation, and (d) after annealing to 8 K. (e) Spectrum after co-deposition of Li atoms and 50:50 H_2/D_2 for 30 min at 4 K, (f) after >470 nm irradiation, (g) after >290 nm irradiation, and (h) after annealing to 7.2 K.

gave small blue-shifts as shown in Figure 3. Annealing the sample first increased the $(LiD)_2$ band by 50%. Bands in the lower region at 446 and 431 cm^{-1} for ^7Li or at 453 and 439 cm^{-1} for ^6Li are not shown.

Mixed isotopic experiments were also performed to help understand the reaction mechanism. Figure 4 compares spectra from ^7Li experiments with HD and a 50:50 H_2/D_2 mixture. Notice the strong Li−H−Li−D absorption at 872.6 cm^{-1} with HD and the weak 869.3 cm^{-1} band for this isotopomer with the mixture. An experiment with ^6Li and HD gave analogous results: the Li−H−Li−D band shifted to 882.6 cm^{-1} and increased by 50% on annealing before photolysis while the analogous $(LiH)_2$ band at 916.1 cm^{-1} increased only 20%.

The absorptions of lithium atom reaction products with H_2 in *para*-hydrogen and with D_2 in *ortho*-deuterium are shown in Figures 5 and 6. The interaction is reduced, which results in
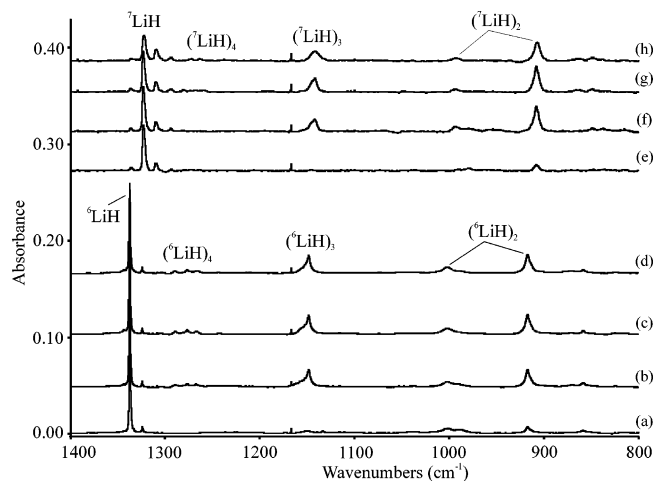

Figure 5. Infrared spectra of lithium atom and *para*-hydrogen reaction products. (a) Spectrum after co-deposition of laser-ablated lithium-6 atoms and 99.9% *para*-hydrogen for 25 min at 4 K, (b) after >470 nm irradiation, (c) after >290 nm irradiation, and (d) after annealing to 7 K. (e) Spectrum after co-deposition of natural Li atoms and 99% *para*-hydrogen for 25 min at 4 K, (f) after >520 nm irradiation, (g) after >380 nm irradiation, and (h) after annealing to 7 K.
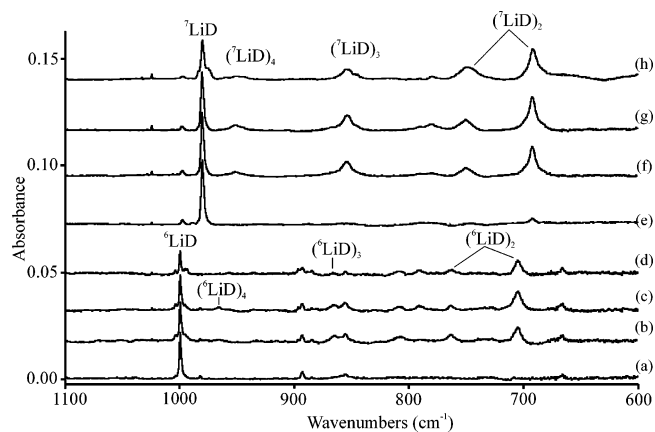

Figure 6. Infrared spectra for lithium atom reaction products with *ortho*-deuterium. (a) Spectrum after co-deposition of laser-ablated enriched lithium-6 atoms and 97% o-D_2 for 25 min at 4 K, (b) after >520 nm irradiation, (c) after >290 nm irradiation, and (d) after annealing to 9 K. (e) Spectrum with natural Li and 94% o-D_2, (f) after >470 nm irradiation, (g) after >290 nm irradiation, and (h) after annealing to 9 K.

slight blue-shifts in both p-H_2 and o-D_2. Note the especially sharp (1.5 cm^{-1} bandwidth) bands for LiH isotopes in the 99.9% p-H_2 sample.

The neon matrix spectra of reaction products of lithium and hydrogen molecules are shown in Figure 7. A very weak band at 909.8 cm^{-1} appeared on the ^7Li atom reaction with H_2 in excess neon during deposition. On >470 nm photolysis, the 909.8 cm^{-1} band increased 10-fold, while new bands appeared at 1270.7, 1151.4, 995.7, 849.6, 571.0, and 560.9 cm^{-1}. On >290 nm photolysis, the 1270.7 cm^{-1} band grew 3-fold, and the 1151.4 and 849.6 cm^{-1} bands increased slightly.

Argon matrix experiments required a substrate temperature near 8 K to obtain reaction products, and only the strongest $(LiH)_2$ absorptions at 900.8 and 909.3 cm^{-1} were observed for the ^7Li and ^6Li reactions with H_2 (Figure 8). These bands shifted to 686.8 and 692.8 cm^{-1} with D_2. A single feature was observed at 868.6 cm^{-1} for ^7Li and HD in solid argon.

Calculations. Electronic structure calculations were performed for the LiH and $(LiH)_n$ molecules and their dihydrogen
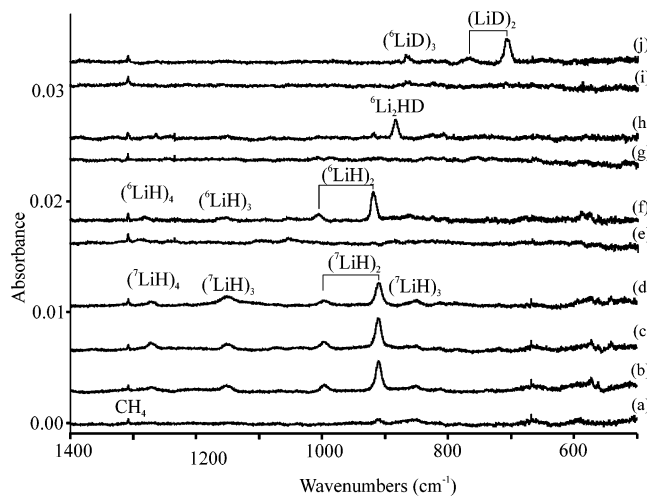
Figure 7. Infrared spectra for lithium atom reaction products with hydrogen isotopes at 3% in excess neon. (a) Spectrum after co-deposition of laser-ablated natural isotopic lithium atoms and H_2 for 60 min at 4 K, (b) after >470 nm irradiation, (c) after >290 nm irradiation, and (d) after annealing to 9 K. (e) Spectrum after co-deposition of enriched lithium-6 atoms and H_2 and (f) after >520 nm irradiation. (g) Spectrum after co-deposition of enriched lithium-6 atoms and HD and (h) after >520 nm irradiation. (i) Spectrum after co-deposition of enriched lithium-6 atoms and D_2 and (j) after >520 nm irradiation.
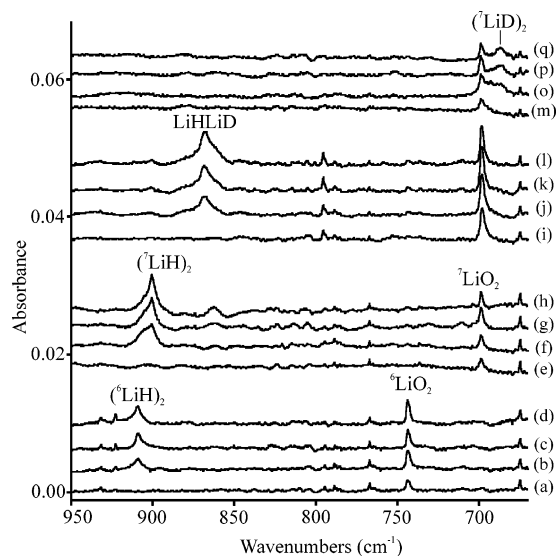

Figure 8. Infrared spectra for lithium atom reaction products with hydrogen isotopes at 5% in excess argon. (a) Spectrum after co-deposition of laser-ablated lithium-6 atoms and H_2 for 60 min at 8 K, (b) after >520 nm irradiation, (c) after 240−380 nm irradiation, and (d) after annealing to 20 K. (e) Spectrum after co-deposition of natural lithium atoms and H_2, (f) after >520 nm irradiation, (g) after 240−380 nm irradiation, and (h) after annealing to 20 K. (i) Spectrum after co-deposition of natural lithium atoms and HD, (j) after >520 nm irradiation, (k) after 240−380 nm irradiation, and (l) after annealing to 20 K. (m) Spectrum after co-deposition of natural lithium atoms and D_2, (n) after >520 nm irradiation, (o) after 240−380 nm irradiation, and (p) after annealing to 20 K.

complexes. Using B3LYP and MP2, the bond lengths of Li−H were predicted to be 1.589 and 1.603 Å, respectively, which are in very good agreement with the gas-phase value of 1.596 Å.[35] The LiH molecule is polarized $Li^{\delta+}-H^{\delta-}$ (calculated natural atomic charges +0.81 and −0.81), and the experimental dipole moment 5.882 D[8] gives 0.77 electron transfer over the bond length in the simple ionic model. Hence, molecular hydrogen can be attached to the dipole ends. Very similar

models were found for $H^-(H_2)_n$ and $H^+(H_2)_n$ clusters.[33] Two conformers, $(H_2)-$LiH (H_2 attached to the Li atom) and LiH−(H_2) (H_2 attached to the H atom) were calculated, and as expected, side-on (H_2)LiH and end-on LiH(H_2) were obtained; however, the side-on form (calculated Li−H fundamental 1404 cm^{-1}) was 0.9 kcal/mol more stable than LiH + H_2, and the end-on was 0.8 kcal/mol less stable at the B3LYP level. The MP2 method gave a higher prediction of complex binding energies, and we computed 3.8 kcal/mol for the $(H_2)-$LiH complex. In addition, we found that two dihydrogen molecules (calculated Li−H fundamental 1404 cm^{-1} or 19 cm^{-1} red-shifted) were bound side-on to Li by 6.7 kcal/mol total and three by 9.5 kcal/mol, so this dipole quadrupole attraction was decreasing per molecule with cluster size. The $(H_2)_2$LiH complex structure in Figure 9 at the B3LYP level is very similar to the MP2 result (0.749, 2.116, 2.014, and 1.598 Å bond lengths and 93.1 and 112.8° angles). At the CCSD(T) level, we find the $(H_2)_n$LiH complexes bound by 2.2, 4.2, and 6.1 kcal/mol total, respectively, so the MP2 method may overestimate the stability of these complexes. Finally, neutral Li and H_2 are repulsive based on our calculations and earlier results.[36] However, polarized LiH activates the complexation of H_2, and more H_2 can be associated to LiH to form larger weak complexes, particularly under the influence of the solid hydrogen matrix cage.

The rhombic ring $(LiH)_2$ and linear Li−H−Li−H dimers have been theoretically investigated, and the former was calculated to be 22 kcal/mol more stable.[14,17,18] Our B3LYP and MP2 calculations reached the same conclusion. We found an imaginary bending mode for the linear dimer in both B3LYP and MP2 calculations using the large basis set, which in fact is a transition state.[18] In contrast, earlier calculations found all real frequencies using a small basis set.[18] The energy favored double-bridge structure dimer Li−$(\mu$-$H_2)$−Li is analogous to HMg−$(\mu$-$H_2)$−MgH and H_2Al−$(\mu$-$H_2)$−AlH_2, and the infrared active Li−H−Li bridge stretching modes are an unambiguous property for such species.[23−25]

Our B3LYP structure for Li−$(\mu$-$H_2)$−Li is illustrated in Figure 9, and the natural charges are +0.84 and −0.84. The MP2 calculation gave similar dimensions (1.760 Å, 80.6°) as did the higher level QCISD (1.765 Å, 80.5°) and CCSD(T) (1.765 Å, 80.6°) computations all using the large Gaussian basis set. Calculated harmonic isotopic frequencies are listed in Table 1 and compared with anharmonic frequencies for the common isotopic molecule. For comparison, the strong IR active modes were +12 and −2 cm^{-1} using MP2 and −4 and −18 cm^{-1} at the QCISD level of theory. In addition, the lithium in $(LiH)_2$ was also polarized, and H_2 molecules associated to form larger complexes. However, only one H_2 can be added to each Li atom in this complex, and this perturbation produced only 1 and 8 cm^{-1} red-shifts from the isolated molecule frequencies. In addition, attempts to calculate a *trans*-Li−H−Li−H isomer again gave the most stable rhombic structure. Finally, earlier calculations for $(LiH)_2$ gave similar structural parameters.[37−39]

Analogous calculations were performed for the LiH trimer and tetramer, and stable cyclic bridged structures were obtained (calculated lithium natural charges +0.81 and +0.80, respectively, with bond lengths of 1.711 and 1.692 Å), which are compared in Figure 9, and the harmonic frequencies are given in Tables 2 and 3. With B3LYP calculations, cyclic $(LiH)_3$ in D_{3h} symmetry is the only stable molecule on the potential energy surface, while three conformers for Li_4H_4 were found. Tetrahedral Li_4H_4 is the lowest in energy (and has a slightly higher +0.81 natural charge), cyclic $(LiH)_4$ in D_{4h} symmetry is 4.7
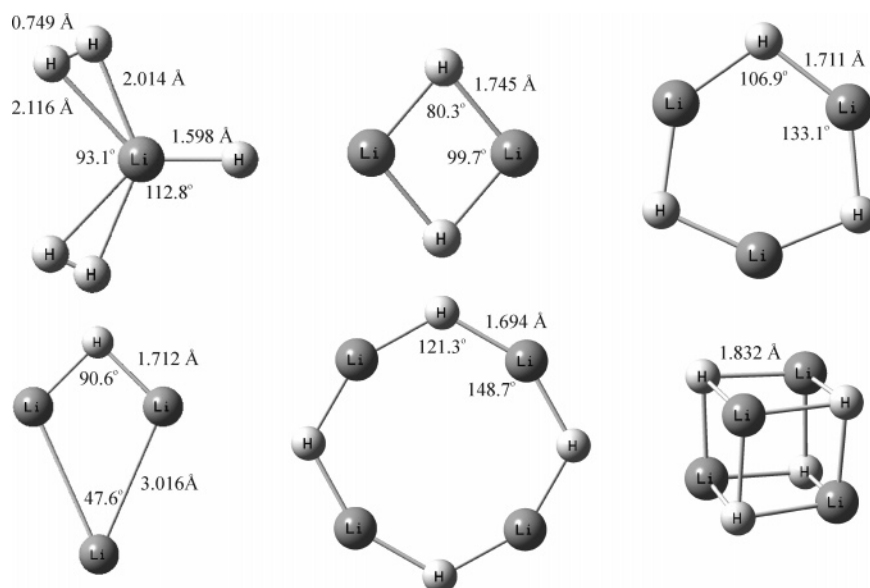
Figure 9. Structures calculated for $(H_2)_2LiH$, $(LiH)_2$, Li_3H, $(LiH)_3$, and $(LiH)_4$ molecules using the B3LYP/6-311++G(3df,3pd) method. Bond lengths in angstroms and bond angles in degrees.

TABLE 1: Infrared Absorptions (cm^{-1}) Observed for Lithium Hydride Diatomic Molecules Complexed and Solvated in Different Hydrogen Matrix Samples

matrix	^{7}LiH	^{6}LiH	matrix	^{7}LiD	^{6}LiD
p-H$_2$, 99.9%	1324.2	1337.4	o-D$_2$, 97%	981.2	998.7
p-H$_2$, 99.8%	1323.9	1337.2	o-D$_2$, 94%	980.3	997.7
p-H$_2$, 99%	1322.9	1336.0			
p-H$_2$, 90%	1319.5	1333.2	o-D$_2$, 80%	980 sh	999 sh
p-H$_2$, 90%	1313	1325.0	o-D$_2$, 80%	979.5	997.5
p-H$_2$, 90%	1304.0	1315.8	o-D$_2$, 80%		996.1
p-H$_2$, 70%	1312.7				
p-H$_2$, 70%	1303.4				
HD	1319.3	1332.5	HD	997.7	1016.2
HD	1309.5	1322.7	HD	989.4	1007.6
n-H$_2$	1309.9	1323.1	n-D$_2$	977.8	995.4
n-H$_2$	1301.2	1314.1			
n-H$_2$/n-D$_2$	1308.2		n-H$_2$/n-D$_2$	989.6	
n-H$_2$/n-D$_2$	1296.8		n-H$_2$/n-D$_2$	980.5	

TABLE 2: Infrared Absorptions (cm^{-1}) Observed for Lithium Hydride Dimer Vibrational Modes in Different Matrix Samples

matrix	(^{7}LiH)$_2$			(^{6}LiH)$_2$		
	b_{1u}	b_{2u}	b_{3u}	b_{1u}	b_{2u}	b_{3u}
neon	909.8	995.7	571.1	919.5	1005.9	
p-H$_2$, 99.9%	908.7			917.4	1002.4	574.6
p-H$_2$, 99%	908.4	993.4				
p-H$_2$, 90%	906.5			914.8		
p-H$_2$, 70%	905.6					
n-H$_2$	904.7	987.1	571.2	913.3	995.7	574.2
argon	900.8			909.3		

kcal/mol higher in energy, and *cis*-Li$_4$H$_4$ lies still 18.9 kcal/mol higher in energy. Our MP2 computation gave very similar results. Earlier SCF calculations gave slightly longer bond lengths with the same trend for these oligomer structures.[37] In like fashion, a stable cyclic (LiH)$_6$ structure was computed in D_{6h} symmetry (bond length of 1.677 Å and highest e mode at 1498 cm^{-1}), but the solid-like hexagonal prism structure (Figure S1) was 18.3 kcal/mol lower in energy.

Discussion

The new product absorptions will be assigned based on argon, neon, normal hydrogen, and *para*-hydrogen matrix infrared spectra and theoretical frequency calculations.

LiH and the $(H_2)_2$LiH Complex. Two very strong absorptions at 1301.2 and 1309.9 cm^{-1} were observed and its matrix site splitting at 1309.9 cm^{-1} were observed after initial deposition of natural lithium with pure normal H$_2$ (n-H$_2$) at 4 K. Sequential irradiation ($>$520, $>$470, $>$380, $>$290, and $>$220 nm from the mercury arc) decreased these bands stepwise. A very weak band at 1323.3 cm^{-1} for ^{6}Li in natural abundance tracks with the two strong bands. The ^{6}Li + n-H$_2$ experiment gave similar 1314.1 and 1323.1 cm^{-1} absorptions, and the ^{6}LiH/^{7}LiH ratios (1.0099 and 1.0101) were close to the computed harmonic value (1.0104) for the diatomic molecules. With normal pure D$_2$ (n-D$_2$), only one counterpart band was found at 977.8 cm^{-1} (^{7}Li) and 995.4 cm^{-1} (^{6}Li), giving isotopic H/D ratios of 1.3307 (^{7}Li) and 1.3202 (^{6}Li), respectively, using the stronger, lower frequency LiH component, which is slightly lower than the harmonic ratios (1.3326 and 1.3221). The pure HD with ^{7}Li experiment revealed two doublets at 1319.3 and 1309.5 cm^{-1} in the Li–H stretching region and 997.7 and 989.4 cm^{-1} in the Li–D stretching region. The ^{6}Li counterparts at 1332.6 and 1322.8 and 1016.2 and 1007.6 cm^{-1} gave lithium 6/7 isotopic frequency ratios of 1.0101 and 1.0102 and 1.0185 and 1.0184, respectively. With H$_2$ + D$_2$ and ^{n}Li, a very similar pattern appeared at 1308.2 and 1296.8 and 989.6 and 980.5 cm^{-1}. The previous isotopic distribution indicates that one hydrogen atom and one lithium atom are involved in this vibration; therefore, an assignment to the diatomic molecule LiH in solid hydrogen is straightforward.

The fundamental vibration of diatomic ^{7}LiH has been measured in the gas phase at 1359.1 cm^{-1},[9] which is much higher than we observed in solid normal hydrogen and indicates a considerable interaction between LiH and surrounding H$_2$ molecules. The assignment to LiH was confirmed by theoretical calculations. With the B3LYP functional, the LiH fundamental was predicted at 1418.9 cm^{-1} (^{7}LiH) and 1433.7 cm^{-1} (^{6}LiH), giving a scale factor of 0.9579 for the gas-phase fundamental. This deviation for the B3LYP harmonic frequency calculation has been found in most metal hydrides.[24–26] Our MP2 calculation gives a slightly higher ^{7}LiH frequency at 1423.2 cm^{-1}, and the higher level QCISD method gave a more accurate frequency of 1364.9 cm^{-1}.[17]

The sharpest and highest LiH fundamentals were observed for ^{7}LiH and ^{6}LiH in 99.9% *para*-hydrogen at 1324.2 and 1337.4

Lithium Hydride Clusters in Solid Hydrogen, Neon, and Argon

J. Phys. Chem. A, Vol. 111, No. 27, 2007 **6013**

TABLE 3: Observed and Calculated Frequencies (cm^{-1}) for (LiH)$_2$ Isotopic Molecules (^1A_g in D_{2h} Symmetry)

mode	(^{7}LiH)$_2$			(^{6}LiH)$_2$		(^{7}LiD)$_2$		(^{6}LiD)$_2$		^{7}Li$_2$HD	
	obsd[a]	calcd an[b]	calcd harm[c]	obsd	calcd harm	obsd	calcd harm	obsd	calcd harm	obsd	calcd harm
a$_g$		1100.7	1174.7(0)		1176.7(0)		841.2(0)		846.0(0)	1076.3	1130.0(386)
b$_{2u}$	987.1	1023.8	1079.5(902)	995.7	1090.7(921)	748.0	810.1(508)	761.5	825.0(527)	872.6	933.8(555)
b$_{1u}$	904.7	913.6	970.9(925)	913.3	981.0(944)	691.0	728.6(521)	703.4	742.0(540)	777.6	823.3(318)
b$_{3g}$		823.2	886.7(0)		899.0(0)		677.8(0)		693.8(0)		698.4(168)
b$_{3u}$	571.2	593.5	600.7(699)	574.2	606.9(714)	446	450.8(394)	453	459.0(408)	497.2	531.0(547)
a$_g$		503.7	522.4(0)		563.3(0)		516.1(0)		554.2(0)		519.4(1)

a Observed frequencies from solid H$_2$, D$_2$, or HD. *b* Calculated anharmonic frequencies at the B3LYP/6-311++G(3df,3pd) level of theory. *c* Calculated harmonic frequencies with infrared intensities in km/mol.
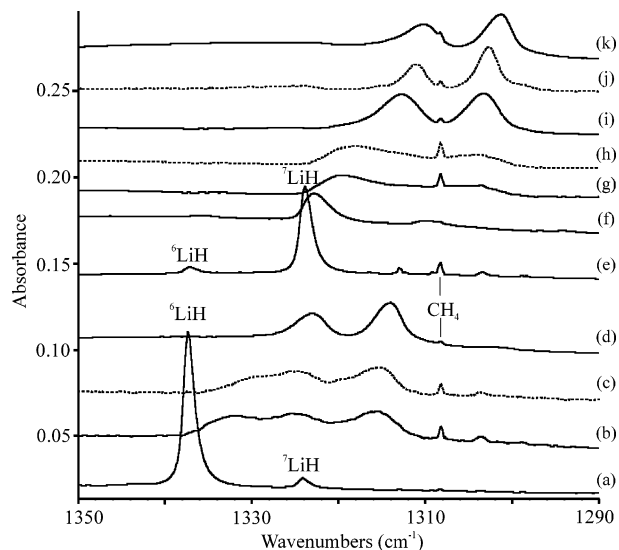

Figure 10. Infrared spectra for LiH in solid hydrogen at 4 K with *para*-hydrogen enrichments ranging from 99.9% to normal hydrogen (25%). (a) ^{6}LiH in 99.9% *para*-hydrogen, (b) ^{6}LiH in 90% *para*-hydrogen, (c) after annealing to 6 K, (d) ^{6}LiH in normal hydrogen, (e) ^{7}LiH in 99.8% *para*-hydrogen, (f) ^{7}LiH in 99% *para*-hydrogen, (g) ^{7}LiH in 90% *para*-hydrogen, (h) after annealing to 6 K, (i) ^{7}LiH in 70% *para*-hydrogen, (j) after annealing to 7 K, and (k) ^{7}LiH in normal hydrogen. Solid spectra are for laser-ablated lithium-6 and natural lithium co-deposited in solid hydrogen samples, and dashed spectra are for annealed samples.

cm^{-1} (ratio 1.0100). However, with 99% *p*-H$_2$, these fundamentals were 1.3−1.4 cm^{-1} lower, and in normal hydrogen (25% para, 75% ortho),[34] these modes were lower still and interestingly split into two bands (Table 1). An analogous finding for LiD fundamentals placed ^{7}LiD and ^{6}LiD highest at 981.2 and 998.7 cm^{-1} in 97% *ortho*-deuterium, and these modes were 0.9−1.0 cm^{-1} lower in 94% *ortho*-deuterium and 2.8−2.3 cm^{-1} lower in normal deuterium (33% para, 67% ortho).[34] The ^{7}LiH/^{7}LiD ratio in the $J = 0$ solids (*p*-H$_2$ and *o*-D$_2$) is 1.3496, and the analogous ^{6}LiH/^{6}LiD ratio is 1.3391, which are slightly higher than the harmonic ratios. The H/D ratios for the two ^{7}LiH and ^{7}LiD sites in the same solid HD, also a quantum solid, are 1.3223 and 1.3235, which are slightly lower than the harmonic value (1.3326) and appropriate for the observed anharmonic frequencies. Likewise, the H/D ratios for the two ^{6}LiH and ^{6}LiD sites in the same solid HD are 1.3114 and 1.3128, respectively, also lower than the harmonic value (1.3221).

Recent work has shown that HCl and DCl rotate in solid *para*-hydrogen with only small deviations from gas-phase behavior.[40] Hence, we must consider this possibility for LiH and LiD in our *para*-hydrogen and *ortho*-deuterium samples. If the strong absorptions we observe were due to R(0) lines, the rotational constants would place the P(1) lines 4 B lower, and our spectra show no evidence of absorption at these positions. The Boltz-

mann populations of $J = 1$ rotational states for ^{7}LiH and ^{7}LiD at 4 K are 0.5 and 5.0%, respectively. Even with the ^{7}LiD absorption at full scale, no signal was detected for the P(1) line anywhere close to 4 B (16.8 cm^{-1}) lower. Hence, we conclude that LiH and LiD are not rotating in these solid hydrogen samples, and we believe that dihydrogen complexes at the metal center are responsible for this quenching of rotational motion.

Earlier workers find that *ortho*-H$_2$ molecules ($J = 1$) with a quadrupole moment that survives averaging over the $J = 1$ rotational wavefunction interact more strongly with guest molecules bearing a dipole moment than *para*-H$_2$ molecules ($J = 0$) where the quadrupole moment averages to zero.[41] In effect, the ortho molecules cluster around the solute molecule due to stronger intermolecular forces. The latter investigation employed CH$_3$F (dipole moment 1.8585 D) as the guest molecule and found an 8.4 cm^{-1} shift for the gas-phase 1048.6 cm^{-1} fundamental in *para*-H$_2$. It is therefore no surprise that ^{7}LiH (dipole moment 5.882 D)[8] is shifted much more in *para*-H$_2$ (34.9 cm^{-1}) from the 1359.1 cm^{-1} gas-phase value.[9] There is a much stronger chemical (or electrostatic) interaction between the highly ionic LiH molecule and the molecular H$_2$ host than found for CH$_3$F. However, Yoshioka and Anderson observed an additional 5.7 cm^{-1} red-shift as 12 *para*-H$_2$ molecules in the matrix cage were replaced by more strongly interacting *ortho*-H$_2$ molecules.[41]

Accordingly, we propose a primary chemical (H$_2$)$_2$LiH complex in the physical cage of a hydrogen lattice substitutional site with 12 surrounding H$_2$ molecules. Thus, the 19.4 cm^{-1} red-shift calculated for this complex at the MP2 level is less than the gas phase to the *para*-H$_2$ shift (34.9 cm^{-1}) because we have not accounted for the solvation of the additional *para*-H$_2$ matrix cage around the complex, which will affect the primary complex formed. Thus, the lower band for ^{7}LiH at 1301.2 cm^{-1} is due to the saturated ortho chemical complex in a physical mostly ortho cage since the more reactive ortho nuclear spin isomer preferentially attaches to guest molecules[41] and our total shift from para to normal (mostly ortho) is a larger 23 cm^{-1}.

This model of a chemical bis-dihydrogen LiH complex in a physical cage of 12 surrounding H$_2$ solvent molecules is in accord with our spectra of LiH in all of the solid molecular hydrogen lattices that we have investigated. To illustrate these effects, we compare infrared spectra from our full range of *para*- and *ortho*-hydrogen samples for both lithium hydride metal isotopic molecules in Figure 10. These spectra begin with the sharp 1337.4 cm^{-1} all-para complex cage absorption for ^{6}LiH, namely, $\{[(J = 0)_2(^6$LiH)]$(J = 0)_{cage}\}$, and the weaker sharp 1324.2 cm^{-1} all-para complex cage band for ^{7}LiH in our most pure (99.9%) para investigation. The corresponding absorptions in solid HD (also a quantum solid with $J = 0$ molecules) are slightly lower at 1332.5 and 1319.3 cm^{-1} (see Table 1) due to the heavier HD cage. However, the 97.9% HD sample contains 2.0% H$_2$, which accounts for the weak bands at 1322.7 and 1309.5 cm^{-1} for $(J = 0)(J = 1)$LiH complexes in the solid HD

lattice. The latter complexes are of course stronger in the normal hydrogen experiments, where the higher bands at 1323.1 and 1309.9 cm^{-1} are then due to the (*para, J* = 0)(*ortho, J* = 1)-LiH complexes, and the lower, stronger bands at 1314.1 and 1301.2 cm^{-1} are assigned to the (*ortho, J* = 1)$_2$LiH complexes. This identification is verified by our 90% para experiments (Figure 10) where now three major broad bands are observed, one for each of the three chemical complexes (*J* = 0)$_2$LiH, (*J* = 0)(*J* = 1)LiH, and (*J* = 1)$_2$LiH. The first band at 1333.2 cm^{-1} for the (*J* = 0)$_2$^{6}LiH complex is of course below the sharp all-para chemical and cage complex band at 1337.4 cm^{-1} owing to the presence of some ortho cage molecules, and the second and third bands at 1325.0 and 1315.8 cm^{-1} are slightly higher than these bands in normal hydrogen due to the presence of more *para*-hydrogen molecules in the cage than in the normal sample (25% para).[34] This is all supported by annealing the sample to 6 K (Figure 10c) where ortho replaces para in the chemical complex (the 1333.2 cm^{-1} band is reduced dramatically and shifted to 1329.6 cm^{-1}) and in the cage around the (*J* = 0)(*J* = 1)LiH and (*J* = 1)$_2$LiH complexes (the bands red-shift slightly to 1324.5 and 1315.3 cm^{-1}). Analogous annealing effects have been reported for CH$_3$F in solid hydrogen.[41]

Similar behavior is found for the (*J* = 0)$_2$^{7}LiH band at 1324.2 cm^{-1} in the mostly lithium-6 sample with 99.9% para, at 1323.9 cm^{-1} in the 99.8% para sample, and at 1322.9 cm^{-1} with 99% para using natural lithium (Figure 10e–g). With 90% para, ^{7}-LiH bands are observed at 1319.5 cm^{-1}, in the middle at 1313 cm^{-1}, and at 1304.0 cm^{-1}, which shift slightly on annealing to 6 K (Figure 10h). The first band appears to be lost using 70% para, and annealing continues to red-shift the bands (Figure 10i,j). As the para concentration is decreased, the band intensity again shifts to lower frequency absorption as the more strongly interacting ortho isomer gradually replaces para (Table 2). Finally, the (H$_2$)$_2$–LiH bonding is strong enough to define a unique bis-dihydrogen–LiH complex, and the *para*- and *ortho*-H$_2$ spin state molecules make a difference in the LiH vibrational frequency in both chemical complex and physical cage roles, and thus, the different hydrogen ligand spin state isomer effects on the Li–H absorptions enable the identification of this bis complex.

The situation is analogous for deuterium except that the shift from the *ortho*-deuterium (*J* = 0) to the normal deuterium (67% ortho)[34] environment is only 3.4 cm^{-1}, and resolving individual peaks for the presumed (D$_2$)$_2$LiD complexes is more difficult. However, the lithium-6 isotope is again easier to resolve, as spectra in Figure 11 demonstrate. The ^{6}LiD absorption in 97% *ortho*-D$_2$ is at 998.7 cm^{-1}, which shifts to 995.4 cm^{-1} in normal deuterium (67% ortho),[34] but with 80% ortho, this feature becomes a weak triplet at the 999 shoulder, 997.5, and 996.1 cm^{-1} (Figure 11d) in the natural abundance spectrum of ^{6}LiD. Annealing to 9 K changes intensities until the 996.1 cm^{-1} peak is the strongest (Figure 11e). The ^{7}LiD absorption shifts from 980.3 to 979.5 to 977.8 cm^{-1} in the analogous spectra with decreasing ortho content (see Table 1). Although the 979.5 cm^{-1} band is not resolved using 80% ortho, it exhibits a 980 cm^{-1} shoulder and shifts to 979.0 cm^{-1} on annealing to 9 K.

Our spectra with mixtures of normal H$_2$ and D$_2$ are in accord with the previous picture. Two bands are now observed using ^{n}Li in the LiD stretching region, at 989.6 and 980.5 cm^{-1}, due to (*J* = 0)(*J* = 1)LiD complexes, and these bands are slightly higher (relative to pure normal deuterium) due to a mass effect from lighter H$_2$ in the cage with D$_2$ molecules. Likewise, the two bands in the LiH stretching region at 1308.2 and 1296.8 cm^{-1} are slightly lower (relative to pure normal hydrogen) due
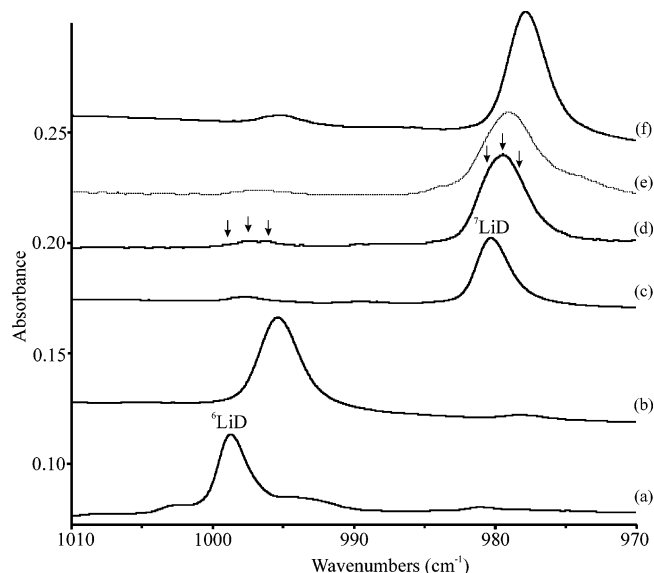

Figure 11. Infrared spectra for LiD in solid deuterium at 4 K with *ortho*-deuterium enrichments ranging from 97% to normal deuterium (67%). (a) ^{6}LiD in 97% *ortho*-deuterium, (b) ^{6}LiD in normal deuterium, (c) ^{7}LiD in 94% *ortho*-deuterium, (d) ^{7}LiD in 80% *ortho*-deuterium, (e) after annealing to 9 K, and (f) ^{7}LiD in normal deuterium. Solid spectra are for laser-ablated lithium-6 and natural lithium co-deposited in solid deuterium samples, and dashed spectra are for annealed samples.

to the presence of heavier D$_2$ in the cage solvation layer with *ortho*-hydrogen.

To summarize, we observed and identified three bis-dihydrogen complexes that differ by the spin states of the two ligands, (*para*)$_2$LiH, (*para*)(*ortho*)LiH, and (*ortho*)$_2$LiH, and the more strongly interacting ortho ligand gives rise to an additional red-shift in the Li–H vibrational chromophore with additional small dependence on the para/ortho composition of the surrounding matrix cage.

The LiH molecule and its hydrogen complex are not observed in our neon and argon matrix experiments, although several laser energies and concentrations of H$_2$ were investigated. This underscores the role of the bis-dihydrogen complex and the hydrogen matrix cage in trapping LiH in solid hydrogen. It further suggests that LiH is extremely reactive and that dimerization and polymerization occur before trapping in the less interacting solid noble gas matrix cage. The (LiH)$_2$ molecule is indeed observed in solid neon as will be discussed next.

(LiH)$_2$. In the ^{7}Li + n-H$_2$ experiments, a group of new bands at 987.1, 904.7, 571.2, and 559.8 cm^{-1} appeared on deposition and tracked together on subsequent treatments of annealing and irradiation. In one experiment, these bands increased 5-fold on >520 nm photolysis, held constant on broadband irradiation down to >290 nm, decreased 50% on >220 nm irradiation, and increased 20% on annealing to 6.9 K. In another sample (Figure 1), annealing first doubled these bands, and >520 nm irradiation increased them by 400%. Substitution with ^{6}Li gave slightly higher absorptions at 995.7 and 913.3 and 574.2 and 564.4 cm^{-1}. With ^{7}Li + n-D$_2$, the two upper bands were observed at 748.6 and 691.2 cm^{-1} (giving 1.3197 and 1.3093 H/D ratios), while the lower bands shifted to 446 and 431 cm^{-1} (1.281 and 1.299 ratios). The counterparts with ^{6}Li + n-D$_2$ were found at 761.5 and 703.4 cm^{-1}, defining 1.3076 and 1.2984 H/D ratios. With ^{7}Li + HD, the diagnostic bands appeared at 1076.3, 872.6 (strongest), 756.1, and 497.2 cm^{-1}. The absorbance yield of this product is much less than that of LiH on deposition, but it exceeds LiH on >520 nm photolysis. The lithium hydride dimer is proposed since the 987.1 and 904.7
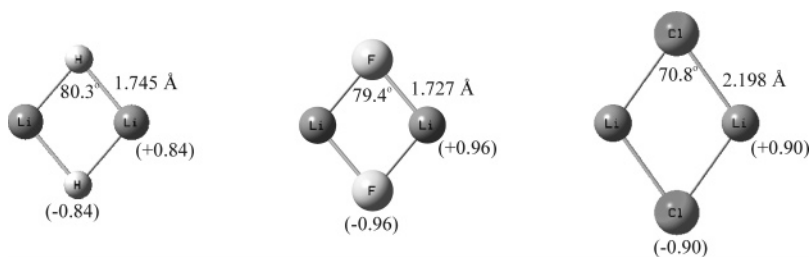
Figure 12. Structures calculated for the isostructural $(LiH)_2$, $(LiF)_2$, and $(LiCl)_2$ molecules using the B3LYP/6-311++G(3df,3pd) method. Bond lengths in angstroms and bond angles in degrees. Natural atomic charges are given in parentheses.

TABLE 4: Observed and Calculated Frequencies (cm⁻¹) for Li₃H₃ (¹A₁′ in D₃ₕ Symmetry)

	$^7Li_3H_3$		$^6Li_3H_3$		$^7Li_3D_3$		$^6Li_3D_3$	
mode	obsd[a]	calcd[b]	obsd	calcd	obsd	calcd	obsd	calcd
e''	1138.0	1229.1 (800 × 2)	1144.0	1240.7 (844 × 2)	852.8	910.0 (532 × 2)	863.3	923.9 (573 × 2)
a_2'		1210.4 (0)		1229.3 (0)		923.4 (0)		944.0 (0)
a_1'		995.6 (0)		995.1 (0)		704.1 (0)		704.2 (0)
e'	843.5	935.6 (458 × 2)	856.0	947.1 (423 × 2)	640.2	711.0 (130 × 2)	(654)	725.9 (101 × 2)
a_2''	538.8	589.1 (955)		594.0 (975)		441.2 (538)		449.3 (558)
a_1'		412.8 (0)		445.0(0)		411.9 (0)		444.8 (0)
e''		326.1 (0)		327.2 (0)		246.3 (0)		252.0 (0)
e'		259.4 (116 × 2)		276.3 (136 × 2)		244.1 (114 × 2)		259.0 (130 × 2)

[a] Observed frequencies from solid normal H_2 or D_2. [b] Calculated harmonic frequencies at the B3LYP/6-311++G(3df,3pd) level of theory with infrared intensities in km/mol.

cm⁻¹ bands are located 300–400 cm⁻¹ lower than the isolated Li−H stretching mode and are appropriate for bridged Li−H−Li stretching vibrations. Very similar shifts from M−H to bridged M−H−M stretching modes have been observed for magnesium dibridged metal hydride, Mg_2H_4, for example.[24] In addition the lithium 6/7 isotopic frequency ratios, 1.0087 and 1.0095, for these modes are almost the same as for the LiH diatomic molecule, which is characteristic of the rhombic dimer.

At this point, a comparison of theoretical calculations and observed values can guide us for assignment. First, the two infrared active Li−H−Li stretching modes for $(LiH)_2$ were computed at 1079.5 and 970.9 cm⁻¹ with B3LYP, which must be multiplied by 0.914 and 0.931 scale factors to fit the bands observed in solid hydrogen. Part of this discrepancy is due to anharmonicity, and part is due to interaction with H_2 molecules in the matrix cage. Accordingly, these scale factors are smaller than typical values for the B3LYP functional.[42] Our MP2 calculation gave similar frequencies of 1076.6 and 982.9 cm⁻¹ and relative intensities (Table S1) as did the BPW91 functional. Second, agreement was also found in deuterium shifts. The slightly lower H/D frequency ratios for the two Li−H−Li stretching motions relative to the Li−H stretching mode are due to more anharmonicity in the bridged bond vibrations. Recall in the cases of dialane (Al_2H_6) and dihydrogen bridged Mg_2H_4 that the bridge bond stretching modes gave slightly higher H/D ratios than the M−H stretching modes since the slightly heavier metal atoms were less involved.[23,24] Third, with B3LYP, the antisymmetric and symmetric modes of Li−(H_2)−Li/Li−(D_2)−Li parallel to the Li−Li axis were calculated at 1079.4 and 810.0 and 1175.0 and 841.4 cm⁻¹, and the modes perpendicular to the Li−Li axis were predicted at 971.4 and 728.9 and 887.0 and 677.9 cm⁻¹. The HD substituted molecule, Li−(HD)−Li, was calculated to give two stronger median bands at 1130.1 and 934.1 cm⁻¹ in the H region and two weaker median bands at 823.1 and 698.6 cm⁻¹ in the D region. The observed 1076.3 and 872.6 (strongest) cm⁻¹ bands in the H region and a weaker 777.6 cm⁻¹ band in the D region were due to Li−H−Li−D. The strongest band shifts to 882.6 cm⁻¹ with ^6Li. Finally, the lower bands at 571.2 and 559.8 cm⁻¹ were assigned to the b_{3u} out-of-plane bending mode split by different interactions with

the matrix (possibly different coordinations of H_2 ligands at the Li centers). The lithium 6/7 isotopic frequency ratios (1.0053 and 1.0082) and the H/D frequency ratios (1.281 and 1.299) for these bands were slightly lower than for the stretching modes, which is probably due to different matrix perturbations in this out-of-plane motion.

Also note (Table 2) that the strongest absorption for the $(LiH)_2$ molecule shifts to lower wavenumbers as the *para*-hydrogen concentration is decreased much the same as described previously for the $(H_2)_2LiH$ complex. The additional red-shift in this absorption from almost pure *para*-hydrogen to normal hydrogen is only about 4 cm⁻¹ as compared to 24 cm⁻¹ for LiH, which can be attributed to the lack of a dipole moment for the $(LiH)_2$ dimer.

The $(LiH)_2$ molecule is also observed in solid neon. After deposition with 3% H_2 in neon, two very weak bands at 909.8 and 995.7 cm⁻¹ appeared, increased on >470 nm photolysis, and decreased on annealing (Figure 7). The ^6Li counterparts at 1005.9 and 919.5 cm⁻¹ define the 1.0103 and 1.0107 6/7 isotopic frequency ratios, respectively, and the $(^6LiD)_2$ absorptions at 768.3 and 706.6 cm⁻¹ give 1.3093 and 1.3013 H/D ratios, which are slightly more harmonic than the frequency ratios in solid hydrogen. These bands correspond to the solid hydrogen observations, and the assignment is straightforward.

In like fashion, the strongest mode was observed to be lower at 900.8 cm⁻¹ in solid argon (Figure 8). Isotopic substitution was performed, and the 6/7 ratio (1.0094) was slightly lower and the H/D ratio (1.3116) slightly higher than found in solid H_2 and D_2. This suggests a stronger interaction of argon at the Li centers with less Li participation in the vibrational mode. The strongest absorption of the Li−H−Li−D isotopomer was observed at 868.6 cm⁻¹ with the same relationship to $(LiH)_2$ as observed in solid HD.

We must point out that all of our calculations (two density functionals, MP2, and QCISD) predicted similar infrared intensities for the strong b_{1u} and b_{2u} modes, but our observed bands are in the ratio of 4:1 in solid neon, 2.5:1 in hydrogen, and 2:1 in *para*-hydrogen (Figures 1, 5 and 7). Part of this discrepancy is due to the harmonic approximations involved, and part is due to the interaction of the ionic Li−(μ-H_2)−Li

TABLE 5: Observed and Calculated Frequencies (cm^{-1}) for Cyclic Li$_4$H$_4$ (^{1}A$_g$ in D_{4h} Symmetry)

	^{7}Li$_4$H$_4$		^{6}Li$_4$H$_4$		^{7}Li$_4$D$_4$		^{6}Li$_4$D$_4$	
mode	obsd[a]	calcd[b]	obsd[a]	calcd[b]	obsd[a]	calcd[b]	obsd[a]	calcd[b]
e$_u$	1274.4	1374.4 (967 × 2)	1282.3	1385.4 (1006 × 2)		1020.6 (597 × 2)		1037.3 (632 × 2)
a$_{2g}$		1361.5 (0)		1378.3 (0)		1032.1 (0)		1054.0 (0)
b$_{1g}$		1341.2 (0)		1342.9 (0)		956.4 (0)		958.9 (0)
a$_{1g}$		873.4 (0)		893.4 (0)		715.0 (0)		746.1 (0)
b$_{2g}$		868.5 (0)		873.6 (0)		618.7 (0)		619.1 (0)
e$_u$		819.6 (632 × 2)		828.3 (598 × 2)		614.9 (215 × 2)		625.5 (183 × 2)
a$_{2u}$		557.3 (1271)		563.1 (1298)		418.2 (716)		425.9 (742)
e$_g$[c]		393.1 (0)		398.0 (0)		298.2 (0)		304.6 (0)

[a] Observed frequencies from solid H$_2$ or D$_2$. [b] Calculated harmonic frequencies at the B3LYP/6-311++G(3df,3pd) level of theory. [c] Another six modes at 326.3(a$_{1g}$,0), 305.9(e$_u$,183 × 2), 210.4(b$_{1u}$,0), 178.7(b$_{2g}$,0), 122.9(b$_{2u}$,0), and 117.1(b$_{1g}$,0).

molecule with the matrix environment. Calculated frequencies with anharmonic correction in the Gaussian 03 system are also compared in Table 1, and of course, the anharmonic frequencies are much closer to the observed values. Unfortunately, the calculation does not provide anharmonic infrared intensities. We have searched the spectra for possible combination bands involving the stretching modes, and no such absorptions are observed. It would be interesting to see if higher levels of theory could account for the observed infrared intensities.

The three IR active fundamentals for (LiH)$_2$ are predicted to have 1:1:0.8 relative intensities, highest to lowest frequency (Table 1), and the observed absorptions are in 1:2.5:1 relative integrated intensities. The best spectrum that we have is for (^{6}LiH)$_2$ in *para*-hydrogen (Figure 5), and the bands at 1002.4 and 917.4 cm^{-1} (fwhm of 11.4 and 5.6 cm^{-1}, respectively) are in a 1.0:1.9 integrated intensity ratio. For the LiHLiD molecule of lower symmetry, the three bands assigned in Figure 2 have 1:10:2 relative integrated intensities, but calculation predicts a 1:1.5:1 relationship. Clearly, the strongest 904.7 and 872.6 cm^{-1} band intensities, which involve H motion parallel to the Li−Li axis, are either underestimated by the calculation or more likely enhanced relatively by the matrix environment. One can picture the (LiH)$_2$ dimer entrapped in the solid hydrogen lattice and the b$_{2u}$ mode (H motion perpendicular to the Li−Li axis) dampened more by the matrix cage than the b$_{1u}$ mode. This point gains credence from the fact that the higher frequency b$_{2u}$ mode absorption is broader (2×) than the lower frequency sharper b$_{1u}$ mode band. We predict that the strongest (LiH)$_2$ fundamental will appear near 910 cm^{-1} in the gas phase and that this mode might be observable by diode laser spectroscopy.

(LiH)$_3$. The LiH trimer can be identified following the assignment of (LiH)$_2$. A strong band at 1138.0 cm^{-1} and a weak band at 843.5 cm^{-1} appeared on >520 nm photolysis, remained constant with further visible and near-UV irradiation, but in contrast to (LiH)$_2$, these bands remained on >220 nm exposure and increased 40% on 6.9 K annealing in ^{7}Li + n-H$_2$ experiments. These bands are also located in the Li−H−Li stretching region. A strong associated 538.8 cm^{-1} band must be the Li−H−Li bending mode. With ^{7}Li + n-D$_2$, the two upper bands shift to 852.8 and 640.2 cm^{-1}, respectively, giving 1.3346 and 1.3176 H/D ratios, and the bending mode shifts out of our measurement region. In experiments with ^{6}Li + n-H$_2$, the bands shift to 1144.0 and 856.0 cm^{-1} (ratios 1.0053 and 1.0148, which are lower and higher than found for the rhombus structure and require a new structure with larger bond angles).

The assignment of (LiH)$_3$ is supported by theoretical calculations. With the B3LYP functional, the optimized D_{3h} ring structure of (LiH)$_3$ gives two IR active degenerate modes at 1229.1 cm^{-1} (in-plane antisymmetric bridge bond stretching modes antisymmetric to C$_2$ axes) and 935.6 cm^{-1} (in-plane antisymmetric bridge bond stretching modes symmetric to C$_2$

axes) and the out-of-plane bending mode at 589.1 cm^{-1} with scale factors 0.926, 0.902, and 0.915, respectively. These scale factors, which are consistent with the calculations for (LiH)$_2$, substantiate the (LiH)$_3$ assignment. The frequencies of (LiD)$_3$ are calculated at 908.0 and 711.5 cm^{-1}, giving 1.3536 and 1.3150 H/D ratios and matching experimental values very well.

Supporting evidence is also obtained from the HD experiments. Two mixed isotopomers, Li$_3$H$_2$D and Li$_3$HD$_2$, are possible for the HD reaction. It must be remembered that solid HD is different from solid H$_2$ and that (LiH)$_2$ itself sustains a 3.2 cm^{-1} blue-shift from the latter to the former environment. The e in-plane antisymmetric bridge bond stretching mode for (LiH)$_3$ calculated at 1232.2 cm^{-1} splits into 1228.0 and 963.0 cm^{-1} bands for Li$_3$H$_2$D and into 1221.4 and 975.7 cm^{-1} bands for Li$_3$HD$_2$. The 1139.8 cm^{-1} band in solid HD is due to Li$_3$H$_3$ as the HD sample contains 2% H$_2$ and the LiH product is expected to diffuse and react more than LiD. The weaker satellite bands at 1132.0 and 1126.0 and at 848.0 and 860.7 cm^{-1}, respectively, are due to Li$_3$H$_2$D and Li$_3$HD$_2$ as these bands increase on >290 nm irradiation with the 1139.8 cm^{-1} band.

(LiH)$_4$. A group of weak bands at 1274.4, 1261.8, and 1252.2 cm^{-1} appeared on >520 nm photolysis and increased on >290 nm photolysis and annealing in n-H$_2$ experiments. The ^{6}Li counterparts at 1282.3, 1269.1, and 1259.1 cm^{-1} defined a 1.0058 ratio, which is near that observed for (LiH)$_3$. For n-D$_2$, a 950.3 cm^{-1} band appeared on >470 nm photolysis, and the H/D ratio 1.3278 is also appropriate. The HD and H$_2$ + D$_2$ reactions favor the upper hydrogen modes. These bands are due to the Li−H−Li bridge bond stretching motions in a larger cluster.

Calculations were performed for Li$_4$H$_4$ and Li$_6$H$_6$, with planar ring and nonplanar bridge structures. For Li$_4$H$_4$, planar D_{4h} and T_d structures (Figure 9) with both B3LYP and MP2 give very different frequencies. The strongest bridged Li−H−Li stretching frequency for the T_d structure is calculated at 926 cm^{-1} since triple bridge interactions are found in this cluster, but for D_{4h}, only double-bridge structures exist, and the strongest frequency shifts up to 1376 cm^{-1}. Similar calculations were performed for Li$_6$H$_6$, and the D_{6h} planar structure also has even higher frequencies. Again, the more solid-like hexagonal prism structure (Figure S1) was lower in energy, but the strongest bridge bond infrared absorptions were calculated as 1127 and 1498 cm^{-1}, respectively, for the prism and planar structures. On the basis of these calculations, we concluded that the 1274.4, 1261.8, and 1252.2 cm^{-1} bands were due to the double-bridge Li−H−Li species (LiH)$_4$ where different matrix sites or numbers of complexing dihydrogen molecules at the lithium centers produced slightly different absorptions. The scale factor (0.917) is comparable to those of the strongest modes for (LiH)$_{2,3}$ (0.931 and 0.926). The matrix apparently prevents the less stable cylic tetramer from folding into the more stable cubic structure.

The *para*-hydrogen lattice interacts less strongly with the $(LiH)_{2,3,4}$ clusters than with the LiH molecule. This is based on the normal to *para*-hydrogen frequency shifts, which are $14-23$ cm^{-1} for LiH, $3.7-4.1$ cm^{-1} for $(LiH)_2$, $4.3-4.5$ cm^{-1} for $(LiH)_3$, and $7.2-7.5$ cm^{-1} for $(LiH)_4$. We believe that this difference is due to the circled-wagon effect, which prevents solvation on the inside of the closed ring structure and of course in part to the lack of a dipole moment for the cyclic $(LiH)_{2,3,4}$ clusters.

Weak Photosensitive Absorption. The weak 981.4 cm^{-1} band is favored relative to LiH with lower laser energy, and it bleaches with visible irradiation to be replaced by the 987.1 cm^{-1} band of $(LiH)_2$. This is the behavior found for PdH_2^- in earlier investigations with laser-ablated Pd and H_2.[43] The [6]-Li counterpart at 991 cm^{-1} and deuterium counterparts at 756 and 743 cm^{-1} for [6]Li and [7]Li, respectively, define isotopic frequency ratios that are compatible with both LiH and $(LiH)_2$ values.
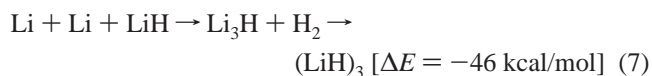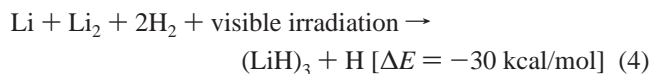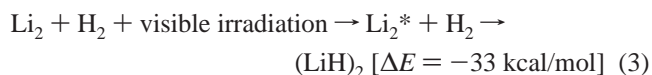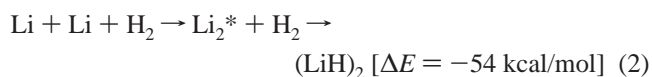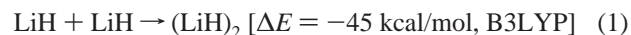
Two possible anions that must be considered for this system are LiH$^-$ and LiH$_2^-$. The first has been observed by photoelectron spectroscopy, and the frequency was estimated from a hot band as 920 ± 80 cm^{-1}.[12] More recently, a first principles theoretical treatment of the photoelectron spectrum has reassigned the hot photoelectron band spectrum and reopened the possibility that the LiH$^-$ vibrational fundamental is near the theoretically predicted harmonic values in the 1100 cm^{-1} region.[44] The second has been computed as a stable linear, centrosymmetric anion with a strong IR active fundamental near 1100 cm^{-1}, a result[36a] in agreement with our B3LYP calculations. However, the lithium 6/7 isotopic frequency ratio for this antisymmetric H$-$Li$-$H stretching mode is computed as 1.0183, which is too high for our observed band. Hence, LiH$^-$ is a possibility with a large matrix shift. Accordingly, we have calculated anion complexes with dihydrogen, and they are repulsive so we must look for another species.

The neutral polylithium Li$_3$H cluster was computed and found to have a cyclic structure as given in Figure 9, and the strongest absorption at 1061.8 cm^{-1} (983 km/mol) was an even better possibility (see Table S2 for all frequencies). This calculated frequency was 7.6% higher than the observed value, which was in line with our other results. Interestingly, both Li$-$H stretching frequencies in Li$_3$H are near the b$_{2u}$ mode of Li$_2$H$_2$. An earlier HF calculation gave slightly longer bond lengths for the cyclic Li$_3$H species.[39] The more important consideration is the mechanism as Li atoms can easily aggregate with LiH and form Li$_3$H, which is expected to be very photosensitive in a hydrogen environment in favor of the stable trimer $(LiH)_3$.

Reaction Mechanisms. The important reaction mechanism is revealed through the use of mixed isotopic reagents. The major product bands on deposition with HD are due to LiH and LiD, and the $(LiH)_2$, LiHLiD, and $(LiD)_2$ molecules are observed as well (Figure 4). There is a preference here for the hydride species over the deuteride species since the HD sample contains 2% H$_2$. Annealing increased the $(LiH)_2$ band by 20% and the LiHLiD band by 50%. Near UV irradiation (>290 nm) increased LiHLiD, Li$_3$H$_2$D, and Li$_3$HD$_2$ more than the other isotopic species. The 50:50 H$_2$/D$_2$ sample gave comparable LiH and LiD bands, more $(LiH)_2$ than $(LiD)_2$, and an intermediate intensity band for LiHLiD. Notice that visible irradiation increased $(LiH)_2$ and $(LiD)_2$ but not LiHLiD. These results show that a small amount of $(LiH)_2$ can be made by dimerization of LiH on sample deposition as given in reaction 1 but that the major growth arises from reactions with the hydrogen molecule reagent. Annealing before irradiation produces $(LiH)_2$ most

probably from spontaneous reaction 2 in solid hydrogen in the $6-7$ K range. Annealing is known to remove lithium atoms, and Li$_2$ is a likely product:[27,28] activation probably arises from the exothermic dimerization of two lithium atoms to give excited Li$_2$*, which spontaneously reduces an adjacent dihydrogen molecule to produce the dilithium dihydride. Annealing also increases the $(LiD)_2$ bands in solid D$_2$ by 50%, which shows that reaction 2 is spontaneous in solid deuterium, although the yield is less than with hydrogen.

Even more growth of $(LiH)_2$ comes from photochemical reaction 3, which excites Li$_2$ directly.[28] We note that red irradiation into the Li atomic absorption does not increase reaction product absorptions, so electronic excitation of atomic lithium in solid hydrogen does not promote chemical reaction with the hydrogen molecule. The major trimer formation also arises on visible irradiation from a reaction such as reaction 4. In addition, the growth of tetramers on annealing at the expense of $(LiH)_{1,2,3}$ probably comes from the exothermic addition reactions 5 and 6. Interactions with H$_2$ molecules in the solid matrix probably prevent the cyclic $(LiH)_4$ molecule from folding into the more stable cubic structure. Finally, the lithium rich cluster Li$_3$H can react with H$_2$ to form the stable cyclic trimer, reaction 7.

$$LiH + LiH \rightarrow (LiH)_2 \; [\Delta E = -45 \text{ kcal/mol, B3LYP}] \quad (1)$$

$$Li + Li + H_2 \rightarrow Li_2^* + H_2 \rightarrow$$
$$(LiH)_2 \; [\Delta E = -54 \text{ kcal/mol}] \quad (2)$$

$$Li_2 + H_2 + \text{visible irradiation} \rightarrow Li_2^* + H_2 \rightarrow$$
$$(LiH)_2 \; [\Delta E = -33 \text{ kcal/mol}] \quad (3)$$

$$Li + Li_2 + 2H_2 + \text{visible irradiation} \rightarrow$$
$$(LiH)_3 + H \; [\Delta E = -30 \text{ kcal/mol}] \quad (4)$$

$$LiH + (LiH)_2 \rightarrow (LiH)_3 \; [\Delta E = -44 \text{ kcal/mol}] \quad (5)$$

$$LiH + (LiH)_3 \rightarrow (LiH)_4 \; [\Delta E = -44 \text{ kcal/mol}] \quad (6)$$

$$Li + Li + LiH \rightarrow Li_3H + H_2 \rightarrow$$
$$(LiH)_3 \; [\Delta E = -46 \text{ kcal/mol}] \quad (7)$$

Bonding. This first experimental observation of the $(LiH)_2$ dimer provides useful information. First, the linear LiH$-$LiH dimer is often considered as the simplest model of the inverse hydrogen bonded complex,[17,18] where the inside H atom is electronically rich and provides electrons and the inside Li atom is electron deficient and accepts them. However, our IR study supports the existence of the more stable rhombic $(LiH)_2$ dimer with the bridging structure, and we do not observe absorption in the 1600 cm^{-1} region that is predicted for the linear dimer. The rhombic dimer structure prevails in metal hydride dimers and polymers, for example, HM$(\mu\text{-H})_2$MH (M = group 2 metals) and H$_2$M$(\mu\text{-H})_2$MH$_2$ (M = group 13 metals).[23-26] This is because the interaction energies involved in the formation of bridging H structures are very large ($30-60$ kcal/mol based on our B3LYP calculations), particularly in an ionic system like $(LiH)_2$, which is much stronger than the typical hydrogen bond.[45] In fact, previous theoretical studies[17,18] have found the linear Li$-$H$-$Li$-$H dimer to be around 22 kcal/mol higher energy than the cyclic $(LiH)_2$ structure, which is consistent with our calculations.

Second, the rhombic $(LiH)_2$ molecule is ionic like the isostructural alkali halide dimers (Figure 11). For example, the

(^{7}LiCl)$_2$ molecule exhibits strong bridge stretching modes at 481.1 and 352.6 cm^{-1}, which are 80.3 and 60.8% of the monomer frequency at 579.5 cm^{-1} in solid argon, and analogous results were found for (^{6}LiCl)$_2$.[46] In like fashion, our (LiH)$_2$ fundamentals are 75.4 and 69.1% of the LiH stretching frequency in solid hydrogen. The LiCl molecule sustained a 10% red-shift in solid argon, whereas the (LiCl)$_2$ molecule appeared to sustain a small blue-shift.[47,48] The LiH molecule was red-shifted 4.2% by the hydrogen matrix as the dipole moment of LiH is smaller than that of LiCl (calculated 5.71 and 6.96 D and observed[8b,49] 5.88 and 7.08 D, respectively), and the basis for matrix interaction is less for LiH. In this regard, the natural charges on Li in (LiCl)$_2$ are +0.90, only +0.84 in (LiH)$_2$, and larger still (+0.96) for (LiF)$_2$, which has almost the same structure as (LiH)$_2$. It is interesting to note that the natural charge on Li in LiH (+0.81) increases in the dimer (to +0.84), but the natural charge on Li in LiCl (+0.94) decreases in the dimer (+0.90). Electrostatic contributions qualitatively account for the dimerization energy in the alkali hydride and halide dimers.[40]

Third, notice the trend in the Li−H bond lengths in the planar cluster series (LiH)$_n$ (see Figures 9 and S1). The longest bond length and lowest Li−H stretching frequency are for the dimer, and the bond length decreases steadily in the cyclic (LiH)$_{3,4,6}$ series, while the stretching frequency increases. Finally, the internuclear distance increases as aggregation becomes three-dimensional, as reported earlier,[38] and the binding energy increases, but the associated Li−H stretching frequency in the solid-like structure decreases.

Conclusion

Laser-ablated lithium atoms and hydrogen gas frozen at 4 K gave the LiH reaction product and trapped Li atoms. The LiH molecule was trapped as the (H$_2$)$_2$LiH chemical complex surrounded by a physical cage of H$_2$ molecules where *ortho*- and *para*-hydrogen played a role in the observed frequencies both in the identification of the primary bis-dihydrogen chemical complex and in the surrounding matrix cage based on spectra recorded with different compositions of *para*- and *ortho*-hydrogen. We are not aware of other examples where the spin state of the dihydrogen ligand is manifest in the complex, but solid hydrogen is an unusual host.

Annealing allows dimerization of Li atoms to Li$_2$*, which reacts spontaneously with H$_2$ in the matrix cage to produce a rhombus structured ionic (LiH)$_2$ dimer. Visible irradiation gives a marked increase in (LiH)$_2$ and new absorptions for (LiH)$_3$. Near UV irradiation and further annealing favor the higher cluster (LiH)$_4$. We observe the simplest possible chemical activation of H$_2$ through the reaction with two Li atoms in solid hydrogen, which can be compared to other synthetic methods using larger chemical systems.[50,51] Finally, the very strong b$_{1u}$ absorption of (LiH)$_2$ is predicted to be near 910 cm^{-1} in the gas phase, where it might be observable by diode laser spectroscopy.

Supporting Information Available: Table of frequencies and figure of structures. This material is available free of charge via the Internet at http://pubs.acs.org.

References and Notes

(1) Dresselhaus, M. S.; Thomas, I. L. *Nature* **2001**, *414*, 332.
(2) Schlapbach, L.; Zuttel, A. *Nature* **2001**, *414*, 353.
(3) Grochala, W.; Edwards, P. P. *Chem. Rev.* **2004**, *104*, 1283.
(4) Balema, V. P.; Wiench, J. W.; Denis, K. W.; Pruski, M.; Pecharsky, V. K. *J. Alloys Compd.* **2001**, *329*, 108.
(5) Kong, V. C. Y.; Kirk, D. W.; Foulkes, F. R.; Hinatsa, J. T. *Int. J. Hydrogen Energy* **2003**, *28*, 205.
(6) Ichikawa, T.; Hanada, N.; Isobe, S.; Leng, H. Y.; Fujii, H. *J. Phys. Chem. B* **2004**, *108*, 7887.
(7) Leng, H. Y.; Ichikawa, T.; Hino, S.; Hanada, N.; Isobe, S.; Fujii, H. *J. Phys. Chem. B* **2004**, *108*, 8763.
(8) (a) James, T. C.; Norris, W. G.; Klemperer, W. *J. Chem. Phys.* **1960**, *32*, 728. (b) Wharton, L.; Gold, L. P.; Klemperer, W. *J. Chem. Phys.* **1960**, *33*, 1255.
(9) Yamada, C.; Hirota, E. *J. Chem Phys.* **1988**, *88*, 6702.
(10) Maki, A. G.; Olson, W. B.; Thompson, G. *J. Mol. Spectrosc.* **1990**, *144*, 257.
(11) Stwalley, W. C.; Zemke, W. T. *J. Phys. Chem. Ref. Data* **1993**, *22*, 87 and references therein.
(12) Sarkas, H. W.; Hendricks, J. H.; Arnold, S. T.; Bowen, K. H. *J. Chem. Phys.* **1994**, *100*, 1884.
(13) (a) Dulick, M.; Zhang, K. Q.; Guo, B.; Bernath, P. F. *J. Mol. Spectrosc.* **1998**, *188*, 14. (b) Bouloufa, N.; Cabaret, L.; Luc, P.; Vetter, R.; Luh, W. T. *J. Chem Phys.* **2004**, *121*, 7237.
(14) Defrees, D. J.; Raghavachari, K.; Schlegel, H. B.; Pople, J. A.; Schleyer, P. v. R. *J. Phys. Chem.* **1987**, *91*, 1857 and references therein.
(15) Bubin, S.; Adamowicz, L. *J. Chem. Phys.* **2004**, *121*, 6249.
(16) Merawa, M.; Begue, D.; Dargelos, A. *J. Phys. Chem. A* **2003**, *107*, 9628.
(17) Rozas, I.; Alkorta, I.; Elguero, J. *J. Phys. Chem A* **1997**, *101*, 4236.
(18) McDowell, S. A. C. *J. Comput. Chem.* **2003**, *24*, 1201.
(19) Wiberg, E.; Amberger, E. *Hydrides of the Elements of Main Groups I–IV*; Elsvier: Amsterdam, 1971.
(20) Wu, C. H.; Jones, R. O. *J. Chem. Phys.* **2004**, *120*, 5128.
(21) Wheeler, S. E.; Sattelmeyer, K. W.; Schleyer, P. v. R.; Schaefer, H. F., III. *J. Chem. Phys.* **2004**, *120*, 4683.
(22) (a) Sannigrahi, A. B.; Kar, T.; Niyogi, B. G.; Hobza, P.; Schleyer, P. v. R. *Chem. Rev.* **1990**, *90*, 1061. (b) Latajka, Z.; Scheiner, S. *J. Chem. Phys.* **1984**, *81*, 4014.
(23) (a) Andrews, L.; Wang, X. *Science* **2003**, *299*, 2049. (b) Wang, X.; Andrews, L.; Tam, S.; DeRose, M. E.; Fajardo, M. *J. Am. Chem. Soc.* **2003**, *125*, 9218. (c) Andrews, L.; Wang, X. *J. Phys. Chem. A* **2004**, *108*, 4202 (Al + H$_2$).
(24) (a) Wang, X.; Andrews, L. *Inorg. Chem.* **2005**, *44*, 610 (Be + H$_2$). (b) Wang, X.; Andrews, L. *J. Phys. Chem. A* **2004**, *108*, 11511 (Mg + H$_2$).
(25) Wang, X.; Andrews, L. *J. Phys. Chem. A* **2004**, *108*, 11500 (Ca, Sr, Ba + H$_2$).
(26) Wang, X.; Andrews, L. *J. Phys. Chem. A* **2005**, *109*, 3849 (Zn, Cd + H$_2$).
(27) Andrews, L.; Pimentel, G. C. *J. Chem. Phys.* **1967**, *47*, 2905.
(28) Fajardo, M. E. *J. Chem. Phys.* **1993**, *98*, 110 and references therein.
(29) Wang, X.; Andrews, L. *Angew. Chem., Int. Ed.* **2007**, *46*, 2602.
(30) Andrews, L. *Chem. Soc. Rev.* **2004**, *33*, 123 and references therein.
(31) (a) Andrews, L.; Wang, X. *Rev. Sci. Instrum.* **2004**, *75*, 3039. (b) The 80 % *ortho*-deuterium sample was prepared by condensing 4 mmol of D$_2$ gas onto our catalyst at 18 K for 2 h.
(32) Kudin, K. N.; Burant, J. C.; Millam, J. M.; Iyengar, S. S.; Tomasi, J.; Barone, V.; Mennucci, B.; Cossi, M.; Scalmani, G.; Rega, N.; Petersson, G. A.; Nakatsuji, H.; Hada, M.; Ehara, M.; Toyota, K.; Fukuda, R.; Hasegawa, J.; Ishida, M.; Nakajima, T.; Honda, Y.; Kitao, O.; Nakai, H.; Klene, M.; Li, X.; Knox, J. E.; Hratchian, H. P.; Cross, J. B.; Adamo, C.; Jaramillo, J.; Gomperts, R.; Stratmann, R. E.; Yazyev, O.; Austin, A. J.; Cammi, R.; Pomelli, C.; Ochterski, J. W.; Ayala, P. Y.; Morokuma, K.; Voth, G. A.; Salvador, P.; Dannenberg, J. J.; Zakrzewski, V. G.; Dapprich, S.; Daniels, A. D.; Strain, M. C.; Farkas, O.; Malick, D. K.; Rabuck, A. D.; Raghavachari, K.; Foresman, J. B.; Ortiz, J. V.; Cui, Q.; Baboul, A. G.; Clifford, S.; Cioslowski, J.; Stefanov, B. B.; Liu, G.; Liashenko, A.; Piskorz, P.; Komaromi, I.; Martin, R. L.; Fox, D. J.; Keith, T.; Al-Laham, M. A.; Peng, C. Y.; Nanayakkara, A.; Challacombe, M.; Gill, P. M. W.; Johnson, B.; Chen, W.; Wong, M. W.; Gonzalez, C.; Pople, J. A. *Gaussian 03*, revision B.04; Gaussian, Inc.: Pittsburgh, PA, 2003, and references therein.
(33) (a) Andrews, L.; Wang, X. *J. Phys. Chem. A* **2004**, *108*, 3879 (H/ H$_2$). (b) Wang, X.; Andrews, L. *J. Phys. Chem A* **2004**, *108*, 1103 (H$^-$/ H$_2$). (c) Andrews, L.; Wang, X. *J. Chem. Phys.* **2004**, *121*, 4724 (D$^+$/D$_2$).
(34) Silvera, I. F. *Rev. Mod. Phys.* **1980**, *52*, 393.
(35) Huber, K. P.; Herzberg, G. *Constants of Diatomic Molecules*; Van Nostrand-Reinhold: New York, 1979.
(36) (a) Boldyrev, A. I.; Simons, J. *J. Chem. Phys.* **1993**, *99*, 4628. (b) Hobza, P.; Schleyer, P. v. R. *Chem. Phys. Lett.* **1984**, *105*, 630.
(37) Rupp, M.; Ahlrichs, R. *Theor. Chim. Acta* **1977**, *46*, 117.
(38) Rao, K. S.; Khanna, S. N.; Jena, P. *Phys. Rev. B* **1991**, *43*, 1416 and references therein.
(39) Kremer, T.; Harder, S.; Junge, M.; Schleyer, P. v. R. *Organometallics* **1996**, *15*, 585.

Lithium Hydride Clusters in Solid Hydrogen, Neon, and Argon

J. Phys. Chem. A, Vol. 111, No. 27, 2007 **6019**

(40) Anderson, D. T.; Hinde, R. J.; Tam, S.; Fajardo, M. E. *J. Chem. Phys.* **2002**, *116*, 594.

(41) (a) Yoshioka, K.; Anderson, D. T. *J. Chem. Phys.* **2003**, *119*, 4731 and references therein. (b) Yoshioka, K.; Anderson, D. T. *J. Mol. Struct.* **2006**, *786*, 12*3*.

(42) (a) Scott, A. P.; Radom, L. *J. Phys. Chem.* **1996**, *100*, 16502. (b) Andersson, M. P.; Uvdal, P. L. *J. Phys. Chem. A* **2005**, *109*, 2937.

(43) Andrews, L.; Wang, X.; Esmail, M.; Manceron, L. *J. Phys. Chem A* **2001**, *105*, 3052.

(44) Chang, D. T.; Reimann, K.; Surratt, G.; Gellene, G. I.; Lin, P.; Lucchese, R. R. *J. Chem. Phys*. **2002**, *117*, 5757.

(45) Scheiner, S. *Reviews in Computational Chemistry, Vol. II*; VCH Publishers: New York, 1991.

(46) Howard, W. F., Jr.; Andrews, L. *Inorg. Chem*. **1975**, *14*, 767.

(47) Klemperer, W.; Norris, W. G. *J. Chem. Phys.* **1961**, *34*, 1071.

(48) Giese, T. J.; York, D. M. *J. Chem. Phys.* **2004**, *120*, 7939.

(49) Lide, D. R., Jr.; Cahill, D.; Gold, L. P. *J. Chem. Phys.* **1964**, *40*, 156.

(50) Welch, G. C.; San Juan, R. R.; Masuda, J. D.; Stephan, D. W. *Science* **2006**, *314*, 1124.

(51) Kubas, G. J. *Science* **2006**, *314*, 1096.